doi:10.1016/j.jmb.2005.09.033 J. Mol. Biol. (2005) 353, 1129–1136

JMB

Available online at www.sciencedirect.com

SCIENCE DIRECT®

ELSEVIER

Visualization of the Phosphorylated Active Site Loop of the Cytoplasmic B Domain of the Mannitol Transporter II^{Mannitol} of the *Escherichia coli* Phosphotransferase System by NMR Spectroscopy and Residual Dipolar Couplings

Jeong-Yong Suh†, Chun Tang†, Mengli Cai and G. Marius Clore*

Laboratory of Chemical Physics Building 5, National Institute of Diabetes and Digestive and Kidney Diseases, National Institutes of Health, Bethesda MD 20892-0520, USA

**Corresponding author*

The solution structure of a stably phosphorylated form of the cytoplasmic B domain of the mannitol-specific transporter (IIB^{Mtl}) of the *Escherichia coli* phosphotransferase system, containing a mutation of the active site Cys384 to Ser, has been solved by NMR. The strategy employed relies principally on backbone residual dipolar couplings recorded in three different alignment media, supplemented by nuclear Overhauser enhancement data and torsion angle restraints related specifically to the active site loop (residues 383–393). As judged from the dipolar coupling data, the remainder of the structure is unchanged upon phosphorylation within the errors of the coordinates of the previously determined solution structure of unphosphorylated wild-type IIB^{Mtl}. Thus, only the active site loop was refined. Phosphorylation results in a backbone atomic rms shift of ~0.7 Å in the active site loop. The resulting conformation is less than 0.5 Å away from the equivalent P-loop in both the low and high molecular mass eukaryotic tyrosine phosphatases. $^{3}J_{NP}$ coupling constant measurements using quantitative *J*-correlation spectroscopy provide a direct demonstration of a hydrogen bond between the phosphoryl group and the backbone amide of Ser391 at position $i+7$ from phospho-Ser384, with an approximately linear P–O–H_N bond angle. The structure also reveals additional hydrogen bonding interactions involving the backbone amides of residues at positions $i+4$ and $i+5$, and the hydroxyl groups of two serine residues at positions $i+6$ and $i+7$ that stabilize the phosphoryl group.

Published by Elsevier Ltd.

Keywords: phosphotransferase system; IIB^{Mannitol}; phosphorylated state; solution structure; NMR

Introduction

The mannitol transporter (II^{Mtl}) of the *Escherichia coli* phosphoenolpyruvate:sugar phosphotransferase system (PTS) is a component of a phosphorelay pathway whereby a phosphoryl group originating on phosphoenolpyruvate is transferred *via* a series of biomolecular steps onto a sugar molecule as it is translocated across the cytoplasmic membrane.[1] Enzyme II^{Mtl} is composed of three domains; the transmembrane C domain (IIC^{Mtl}) at the N terminus, followed by two cytoplasmic domains, B (IIB^{Mtl}) and A (IIA^{Mtl}), connected by long (38 and 33 residues) flexible linkers.[1,2] IIA^{Mtl} accepts the phosphoryl group from the histidine-containing phosphocarrier protein HPr and transfers it to IIB^{Mtl}. IIC^{Mtl} catalyzes the translocation of mannitol across the membrane and its concomitant phosphorylation by IIB^{Mtl}. We have previously solved

† J.-Y.S. and C.T. contributed equally to this work.

Abbreviations used: PTS, phosphotransferase system; Mtl, mannitol; HPr, histidine-containing phosphocarrier protein; II^{Mtl}, mannitol transporter; IIA^{Mtl}, IIB^{Mtl} and IIC^{Mtl}, A, B and C domains, respectively, of II^{Mtl}; NOE, nuclear Overhauser effect; RDC, residual dipolar coupling; HSQC, heteronuclear single quantum coherence; rms, root-mean-square.

E-mail address of the corresponding author: mariusc@intra.niddk.nih.gov

0022-2836/$ - see front matter Published by Elsevier Ltd.

the solution structures of the IIA^{Mtl}-HPr complex[3] and IIB^{Mtl}.[4] Despite the absence of any significant sequence identity, we showed that the fold of IIB^{Mtl} is remarkably similar to that of the low molecular mass eukaryotic tyrosine phosphatases (which contain two long insertions relative to IIB^{Mtl}),[5] as well as to that of enzyme IIB^{Chitobiose},[6] a component of the *N*,*N*′-diacetylchitobiose branch of the PTS. Moreover, the backbone conformation of the active site loop, which contains a cysteine residue that is phosphorylated, is similar to that of both the low[5] and high[7] molecular mass tyrosine phosphatases. Phosphorylated IIB^{Mtl} is not sufficiently stable to permit structural studies. However, it has been shown recently that mutation of the active site cysteine residue to serine (C384S) yields a protein that can be stably phosphorylated.[8] Here, we present the structure of the phosphorylated form of the C384S mutant of IIB^{Mtl} and elucidate the interactions responsible for stabilizing the phosphoryl group.

Results and Discussion

RDCs for phospho-IIB^{Mtl}(C384S)

A comparison of the measured $^1D_{NH}$, $^1D_{NC'}$ and $^2D_{HNC'}$ residual dipolar couplings (RDCs) recorded in three different alignment media (phage pf1, neutral gel and positive gel) on phospho-IIB^{Mtl}(C384S) and those calculated from the previously determined solution NMR structure of unphosphorylated IIB^{Mtl}[4] reveals excellent agreement, with the exception of a few RDCs involving residues 386–391 in the active site loop (Figure 1 and Table 1). The three alignment tensors are significantly different from one another, as indicated by low values of the scalar tensor products:[9] 0.73, −0.52 and 0.02 between the alignment tensors in pf1 and neutral gel, pf1 and positive gel, and neutral and positive gels, respectively. In addition, these three alignment tensors differ significantly from that of the alignment tensor in a polyethylene glycol(PEG)/hexanol liquid crystalline medium used to refine the structure of unphosphorylated IIB^{Mtl} (scalar tensor products of 0.86, 0.77 and −0.14 *versus* the current alignment tensors in neutral gel, pf1 and positive gel, respectively).[4] Consequently, the combined RDC data in the three alignment media used here provide stringent restraints on the relative orientations of the backbone N–H, N–C′ and H_N–C′ vectors, and hence serve both to validate the structure of unphosphorylated IIB^{Mtl} and to ascertain unambiguously regions where significant perturbations in the backbone occur upon phosphorylation. With the RDCs for the outlying residues within the active site loop omitted, the dipolar coupling *R*-factors[10] for the N–H RDCs measured in phage pf1, neutral gel and positive gel are 16.0%, 14.7% and 23.3%, respectively. (Note the larger value for the latter is simply due to the larger relative error in the measured RDCs owing to the low degree of alignment in the positive gel; see Table 1). These values lie within the range expected for 1.5–2 Å resolution crystal structures.[11,12] One can therefore conclude that within the errors of the NMR coordinates of IIB^{Mtl}, the only backbone conformational changes that occur upon phosphorylation are located within the active site loop encompassing the phosphorylated residue at position 384, which is serine in the current construct and cysteine in the wild-type protein.

Direct observation of a hydrogen bond to the phosphoryl group

Direct demonstration of electron orbital overlap

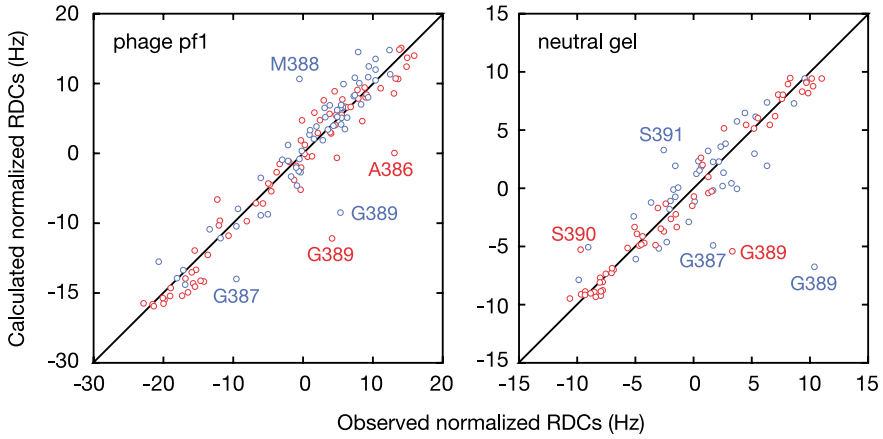

Figure 1. Comparison of observed RDCs for phospho-IIB^{Mtl}(C384S) with those calculated from the coordinates of unphosphorylated wild-type IIB^{Mtl} in two alignment media. The N–H and normalized N–C′ RDCs are shown in red and blue, respectively, in two alignment media (phage pf1 in the left-hand panel, and neutral gel in the right-hand panel). Residues where the observed and calculated RDCs differ significantly are labeled; these involve residues 386–391 within the active site loop. The $^1D_{NC'}$ RDCs are normalized to the same scale as the $^1D_{NH}$ RDCs by multiplying the observed $^1D_{NC'}$ RDCs by the factor $\gamma_H r^3_{NC'}/\gamma_C r^3_{NH}$, where γ_H and γ_C are the gyromagnetic ratios of hydrogen and carbon, respectively, and $r_{NC'}$ and r_{NH} are the N–C′ and N–H bond lengths, respectively.

Table 1. Dipolar coupling *R*-factors for RDCs measured on phospho-IIB^{Mtl}(C384S) in multiple alignment media

	Dipolar coupling *R*-factor (%)[a]						
	Phage pf1			Neutral gel			Positive gel
	$^1D_{NH}$	$^1D_{NC'}$	$^2D_{HNC'}$	$^1D_{NH}$	$^1D_{NC'}$	$^2D_{HNC'}$	$^1D_{NH}$
Unphosphorylated IIB^{Mtlb}							
All	23.1	23.5	32.7	23.4	51.3	48.3	26.8
Outliers omitted[c]	16.0	15.7	21.9	14.7	28.9	27.5	23.3
Active site[d]	47.3	41.4	55.9	46.2	108.8	101.0	42.2
Phospho-IIB^{Mtl}(C384S)[e]							
All	14.4	15.1	21.9	13.3	29.4	26.1	20.2
Active site[d]	5.7	12.7	13.3	15.6	35.1	24.9	11.7

[a] The dipolar coupling *R*-factor, which scales between 0% and 100%, is defined as the ratio of the rms deviation between observed and calculated values to the expected rms deviation if all the bond vectors were distributed randomly.[10] The latter is given by $\{2D_a^2[4+3\eta^2]/5\}^{1/2}$, where D_a is the magnitude of the axial component of the alignment tensor and η is the rhombicity. The values of D_a^{NH} and η, obtained by singular value decomposition, using the coordinates of unphosphorylated IIB^{Mtl},[4] and excluding outlying data for residues 386–391 (see footnote c) are −11.0 Hz and 0.27, respectively, in phage pf1; −4.8 Hz and 0.65, respectively, in the neutral gel, and 3.8 Hz and 0.42, in the positive gel. The small degree of alignment in the positive gel precluded accurate measurement of $^1D_{NC'}$ and $^1D_{HNC'}$ RDCs.

[b] Coordinates of regularized mean structure of wild-type unphosphorylated IIB^{Mtl} from Legler *et al.*[4] (PDB accession code 1VKR).

[c] The following outlying data (see Figure 1) involving residues 386–391 within the active site were omitted: N–H RDCs for residues 386 and 389 in pf1, 389 and 390 in the neutral gel, and 386, 387 and 389 in the positive gel; N–C′ RDCs for residues 387, 388 and 389 in phage pf1, and residues 387, 389 and 391 in the neutral gel; and HNC′ RDCs for residues 386–389 in phage pf1, and residue 389 in the neutral gel.

[d] Residues 383–393.

[e] Restrained regularized mean coordinates (this work).

across a hydrogen bond can be demonstrated by the observation of scalar couplings between donor and acceptor atoms.[13] The difference spectrum between the ^{31}P decoupled and coupled ^{1}H–^{15}N constant time heteronuclear single quantum coherence (HSQC) spectra[14] reveals the presence of a single cross-peak corresponding to the backbone amide of Ser391. The ratio of the cross-peak intensities in the two spectra is given by $\cos(\pi^3J_{NP}T)$, where T is the coupling evolution period (100 ms) and $^3J_{NP}$ is the three-bond scalar coupling across the hydrogen bond between the nitrogen atom of the donor and the phosphorus atom of the acceptor. The measured $^3J_{NP}$ coupling constant is 1.7 Hz. Previous work has shown that the observation of a measurable $^3J_{NP}$ coupling is related to the distance (<3 Å) between the nitrogen and oxygen atoms of the donor and acceptor groups, and to the P–O–H_N angle.[14] For an angle close to 180°, the $^3J_{NP}$ coupling is around 4–5 Hz, while for angles less than 120° the value drops to less than 0.4 Hz. One can therefore conclude that the P–O–H_N(Ser391) angle across the hydrogen bond in phospho-IIB^{Mtl}(C384S) is approximately linear. This information can be incorporated into the structure refinement in the form of a loose, weak, angle restraint.

Refinement of the active site loop

On the basis of the RDC data discussed above, we proceeded to refine the structure of the active site loop (residues 383–393) using torsion angle simulated annealing with RDC restraints, supplemented by NMR-derived approximate interproton distance and torsion angle restraints involving the active site residues. The coordinates of all residues outside the active site loop were held fixed to their positions in the previously determined structure of unphosphorylated IIB^{Mtl}.[4] A summary of the structural statistics is provided in Tables 1 and 2, and a superposition of the 150 calculated simulated annealing structures is shown in Figure 2(a).

The atomic rms difference between the individual simulated annealing structures and the mean coordinates for the active site loop is 0.06 Å for the backbone (N, C^α, C, O) atoms and 0.65 Å for all heavy atoms. While the side-chains of phospho-Ser384 and Ser390 are defined uniquely in a single rotameric state (both g^+), the side-chains of Asp385, Met388, Ser391 and Met393 in the calculated structures are rotamer averaged. Asp385 samples the t ($\chi_1 = 179.2(\pm 1.6)°$) and g^+ ($\chi_1 = 58.5(\pm 1.7)°$) rotamers approximately equally; Ser391 is predominantly in the g^+ rotamer (75% with $\chi_1 = 64(\pm 7)°$), with minor, approximately equally populated, skewed t ($\chi_1 = -157(\pm 1)°$) and g^- ($\chi_1 = -94(\pm 3)°$) rotamers. In both cases, degeneracy of the H^β proton chemical shifts precluded a definitive rotamer assignment based on the nuclear Overhauser effect (NOE) data. However, several observations suggest that the rotameric states of Asp385 and Ser391 can be assigned on stereochemical and chemical grounds. In the g^+ rotamer, the carboxylate group of Asp385 is <2.9 Å from an oxygen atom of the phosphoryl group. Thus, unless the carboxylate group of Asp385 is protonated, electrostatic repulsion between the two negatively charged groups would exclude the g^+ rotamer. The observation that the minor rotamers of Ser391 are skewed suggests that Ser391 is, in all likelihood, exclusively in the t rotamer. Skewing of the g^+ and t rotamers of Ser391 is due to steric clash with the side-chain oxygen atom of Ser384 and the backbone carbonyl oxygen atom of Val382, respectively.

Table 2. Structural statistics

	⟨SA⟩	$(\overline{SA})_r$
Number of experimental NMR restraints		
Distances[a]	97	
Torsion angles[a]	21	
RDCs in phage pf1[b]		
$^1D_{NH}$	75 (11)	
$^1D_{NC'}$	59 (11)	
$^2D_{HNC'}$	58 (11)	
RDCs in the neutral gel[b]		
$^1D_{NH}$	75 (11)	
$^1D_{NC'}$	59 (6)	
$^2D_{HNC'}$	58 (6)	
RDCs in the positive gel[b]		
$^1D_{NH}$	75 (10)	
rms deviation from distance restraints[c] (Å)	0.005 ± 0.002	0.005
rms deviation from side-chain torsion angle restraints[c] (deg.)	0.39 ± 0.09	0.50
Coordinate precision of the active site (residues 383–393)[d] (Å)		
Backbone (N, C$^\alpha$, C′, O) atoms	0.06 ± 0.02	
All heavy atoms	0.65 ± 0.09	

The notation of the NMR structures are as follows: ⟨SA⟩ are the final 150 simulated annealing structures, $(\overline{SA})_r$ is the restrained regularized mean structure. Note, only the coordinates of the active site (residues 383–393) are refined (see the text).

[a] The number of distance and torsion angle restraints relate specifically to the active site residues 383–393, whose coordinates were refined. There are 83 NOE-derived interproton distance restraints that involve at least one active site residue: eight intraresidue, and 17 sequential ($|i-j|=1$), 20 medium range ($1<|i-j|\leq 5$), and 38 long-range ($|i-j|>5$) interresidue restraints. These are supplemented by 12 restraints for six backbone hydrogen bonds (involving one active site residue) within regions of regular secondary structure, and two restraints for the hydrogen bond between the backbone amide of Ser391 and the phosphoryl group for which there was an observable $^3J_{NP}$ scalar coupling. The loose torsion angle restraints comprise ten ϕ, nine ψ and two χ_1 angles.

[b] The first number refers to the total number of RDCs measured, while the number in parentheses refers specifically to the number of residues within the active site (residues 383–393). The average dipolar coupling *R*-factors for the ensemble of 150 simulated annealing structures is the same as that for the restrained regularized mean coordinates provided in Table 1.

[c] None of the structures exhibits distance violations greater than 0.1 Å or torsion angle violations greater than 3°.

[d] Defined as the average rms difference between the final 150 simulated annealing structures and the mean coordinates.

Consequently, the rotameric states of Asp385 and Ser390 were restrained to the *t* and g^+ conformations in the calculation of the restrained regularized mean coordinates.

A comparison of the active site loop in the phosphorylated and unphosphorylated states is shown in Figure 2(b). The low dipolar coupling *R*-factors for the residues within the active site (residues 383–393) of phospho-IIB^{Mtl}(C384S) indicate that the RDCs in all three alignment media recorded on phospho-IIB^{Mtl}(C384S) are satisfied within experimental error upon structure refinement (Table 1). By way of contrast, the RDCs recorded in PEG/hexanol on unphophorylated IIB^{Mtl}[4] fit only poorly to the active site residues of the refined structure of phospho-IIB^{Mtl}(C384S) with $^1D_{NH}$, $^1D_{NC'}$ and $^2D_{NC'}$ dipolar coupling *R*-factors of 21.8%, 38.7% and 58.4%, respectively, compared to 5.9%, 17.8% and 23.8%, respectively, for the structure of unphosphorylated IIB^{Mtl}.[4] The overall backbone (N, C$^\alpha$, C, O) atomic rms shift between the two states for residues 383–393 is 0.67 Å with the largest displacements involving Ala386 and Met388. These relatively small changes in backbone conformation are sufficient to satisfy the RDCs recorded in the three media. The most significant changes in backbone torsion angles involve ψ of Met388 and ϕ of Gly389, which shift from −68° and −31°, respectively, in the unphosphorylated state, to 10° and −131°, respectively, in the phosphorylated form. The ϕ/ψ angles for both these residues remain within the additionally allowed regions of the Ramachandran plot in both forms.[15]

Stabilization of the phosphoryl group within the active site

The active site loop together with the side-chains of spatially adjacent residues that make contact with the loop is displayed in Figure 3. The conformation of the active site loop is stabilized both by interactions within the loop and hydrophobic contacts with side-chains outside the loop. In particular, the C$^\delta$ methyl group of Ile417 is packed against the methyl group of Ala383 and the backbone of Ser384 and Asp385; the methyl group of Ala416 is packed against the backbone of Ala386; the methyl groups of Leu69 are packed against the backbone of Ser384 and Asp385, as well as the β-methylene group of Asp385; and the aromatic ring of Phe452 is in direct contact with the β-methylene group of Ser390.

Several hydrogen bonds from backbone amide groups to the phosphoryl group and oxygen atom of Ser384 stabilize phospho-Ser384. These hydrogen bonds are characterized by N–O and H_N–O distances <2.6 Å and <2 Å, respectively. The phosphoryl group is hydrogen bonded to the backbone amides of Met388, Gly389 and Ser391, at positions $i+4$, $i+5$ and $i+7$, respectively, from phospho-Ser384. The P–O–H_N angle is 166° for Ser391 but only 136° and 103°, for Met388 and Gly389,

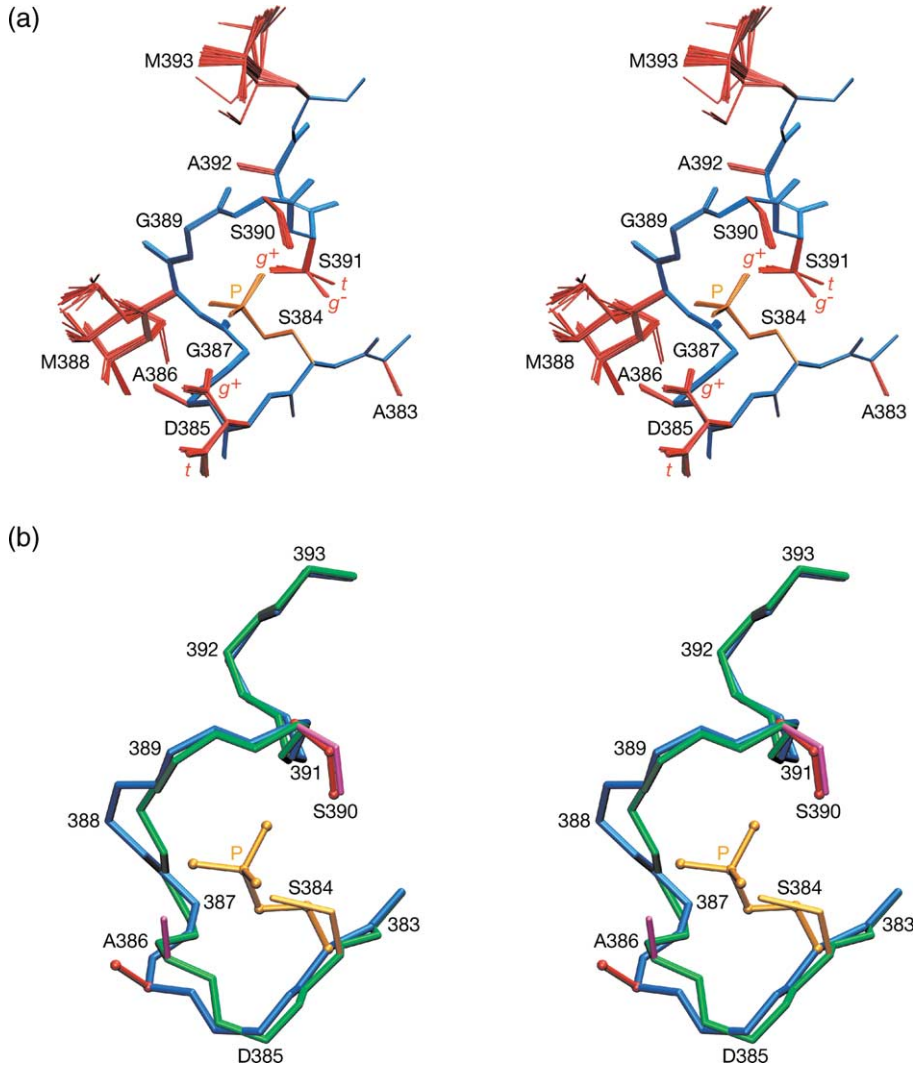

Figure 2. Structure of the active site loop of phospho-IIB^{Mtl}(Cys384S). (a) Stereoview of a superposition of 150 simulated annealing structures with the backbone (N, C$^{\alpha}$, C, O) atoms in blue and the side-chains in red. Note the multiple rotameric states for Asp-385 (g^+ or t), Met388, Ser391 (predominantly t) and Met-393. (b) Stereoview of a best-fit superposition of the active site of phospho-IIB^{Mtl}(C384S) and unphosphorylated IIB^{Mtl}, with the backbone (N, C$^{\alpha}$, C) atoms in blue and green, respectively, and selected side-chains in red and purple, respectively. Phospho-Ser384 and unphosphorylated Cys384 are shown in gold. The coordinates of the restrained regularized mean coordinates are shown.

respectively, thereby accounting for the observation that a *trans*-hydrogen bond $^3J_{NP}$ coupling is observed only for Ser391. The phosphoryl group is also hydrogen bonded to side-chain donor groups: a phosphoryl oxygen atom is <2.8 Å from the hydroxyl oxygen atom of Ser390, and ~ 3.1 Å from the hydroxyl oxygen atom of Ser390 in the t rotamer. Finally, the backbone amide of Gly387 is hydrogen bonded to the oxygen side-chain atom of Ser384. This serves to make the latter more nucleophilic, thereby promoting phosphorylation and stabilizing the O(Ser384)–P bond.

We previously pointed out that residues 384–391 of unphosphorylated IIB^{Mtl} adopt a similar conformation to that of the P-loop of a trapped cysteinyl-phosphate intermediate of a high molecular mass protein tyrosine phosphatase[7] and a vanadate transition state complex of a low molecular mass protein tyrosine phosphatase.[5] The backbone of residues 384–391 (CDAGMGSS) of unphosphorylated IIB^{Mtl} can be superimposed on the equivalent residues of these two tyrosine phosphatases (residues 215–222, CSAGIGRS, and residues 12–19, CLGNICRS, respectively) with C$^{\alpha}$ atomic rms differences of 0.6 Å and 0.9 Å, respectively. Upon phosphorylation of IIB^{Mtl}, structural convergence is further increased and these differences are further reduced to only 0.4 Å and 0.5 Å, respectively.

It is interesting to speculate on the potential role of Asp385. In unphosphorylated IIB^{Mtl}, Asp385 appears to adopt both the t and g^+ conformations.[4] While we cannot distinguish between these two conformers on the basis of the experimental NMR data for phospho-IIB^{Mtl}(C384S), it is evident that the g^+ rotamer of Asp385 would result in electrostatic repulsion between the negatively charged

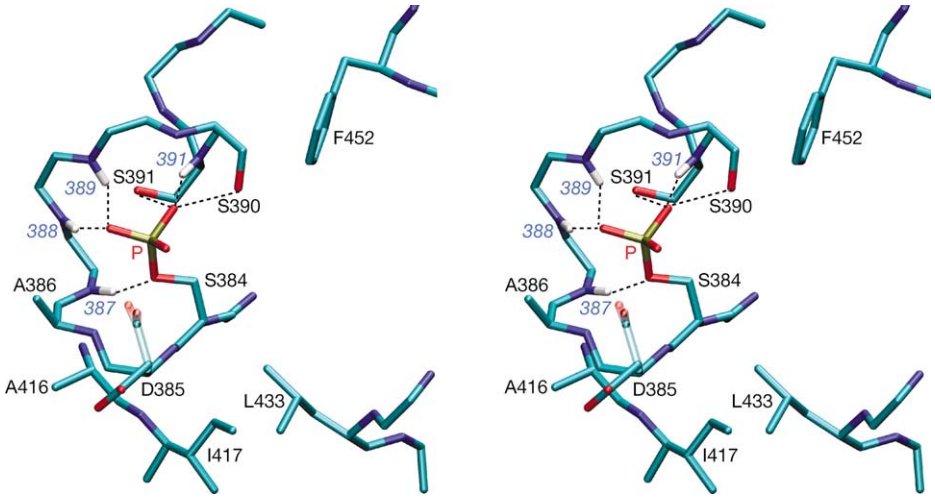

Figure 3. Hydrogen bonding within the active site loop of phospho-IIB^{Mtl}(C384S). Hydrogen bonds are indicated by broken black lines. Asp385 is shown in both the *t* (solid) and g^+ (transparent) rotamers. Side-chains outside the active site loop that are in contact with the active site are also displayed. Color coding is according to atom type with carbon in cyan, oxygen in red, nitrogen in blue, phosphorus in gold and backbone amide protons in white. Backbone amide protons involved in hydrogen bonding with phospho-Ser-384 are labeled in blue italics.

carboxylate and phosphoryl groups, thereby destabilizing the phosphorylated state. Hence, the occurence of the g^+ rotamer for Asp-385 in free phospho-IIB^{Mtl}(C384S) is highly unlikely. In the context of phosphoryl transfer from IIA^{Mtl} to IIB^{Mtl}, it seems likely that the negatively charged carboxylate group of Asp385 would be neutralized by interaction with a positively charged residue of IIA^{Mtl}, probably the conserved Arg49, which is in close proximity to the active site His65.[3] In the case of the IIB^{Mtl}–IIC^{Mtl} complex, however, the phosphoryl group residing on Cys384 is transferred onto the incoming mannitol molecule that is translocated across the membrane through the integral membrane component IIC^{Mtl}. It is possible, therefore, that Asp385 could act as a molecular switch, promoting the dissociation of the phosphoryl group from Cys384 of IIB^{Mtl} upon adoption of the g^+ rotameric state.

Concluding remarks

Using a comprehensive set of backbone RDCs recorded in multiple alignment media, we have been able to demonstrate that phosphorylation of IIB^{Mtl} is accompanied by conformational changes that are localized specifically to the active site loop. The availability of data for several backbone vectors in multiple alignment media permits the backbone of the active site loop in the phosphorylated state to be defined with great accuracy. The resulting structure of the active site loop, whose backbone is remarkably similar to that of the P-loop of eukaryotic tyrosine phosphatases, provides a set of hydrogen bond donors, comprising the backbone amide group of the residues at positions $i+4$, $i+5$ and $i+7$, and the hydroxyl groups of the serine residues at positions $i+6$ and $i+7$ that stabilize the phosphorylated state. The present structure of phospho-IIB^{Mtl}(C384S) provides a basis for extending this work to a complex representing a transition state intermediate between the A and phosphorylated B domains of II^{Mtl}.

Experimental

Cloning, expression and purification of phospho-IIB^{Mtl}(C384S)

The original clone of the IIB^{Mtl} domain,[4] encompasing residues 366–489 of full-length II^{Mtl}, was modified to generate a new construct encoding residues 375–476 (plus Gly-Ser at the N terminus as a thrombin cleavage site) with a single mutation of Cys384 to Ser. This shorter construct (verified by DNA sequencing) in which the disordered N and C-terminal regions have been removed, was subcloned into a modified pET-32a vector[4] to form a thioredoxin fusion protein with a His_6 tag. $^{15}N/^{13}C$-labeled IIB^{Mtl}(C384S) was expressed and purified as described.[4] Phosphorylation was carried out essentially as described:[8] 193 μM IIB^{Mtl}(C384S) was incubated at 37 °C in 20 mM Tris (pH 7.4), 1 mM EDTA, 5 mM $MgCl_2$, 10 mM phosphoenolpyruvate, 1.93 μM enzyme I,[16] 3.87 μM HPr[3] and 3.87 μM IIA^{Mtl3} for 3 h. Phospho-IIB^{Mtl}(C384S) was eluted on a Mono Q anion-exchange column with a 0–1 M NaCl gradient. Phosphorylation was confirmed by mass spectrometry and native gel electrophoresis. Purity was greater than 98%. NMR samples contained 0.8 mM [*U*-$^{15}N/^{13}C$]-phospho-IIB^{Mtl}(C384S) in 20 mM Tris-d_{11} (pH 7.4), 0.01% (w/v) sodium azide and either 90% H_2O/10% ^2H_2O or 99.996% ^2H_2O.

NMR spectroscopy

NMR spectra were collected at 30°C on Bruker DMX600, DRX600 and DMX750 spectrometers equipped with an *x,y,z*-shielded gradient quadruple resonance probe, a *z*-shielded gradient triple resonance cryoprobe and an *x,y,z*-shielded gradient triple resonance probe, respectively. Spectra were processed with the NMRPipe package,[17] and analyzed using the programs PIPP/CAPP/STAPP.[18]

Sequential and side-chain assignments of phospho-IIB^{Mtl}(C384S) were performed using 3D triple resonance through-bond scalar correlation experiments (3D HNCACB, CBCA(CO)NH, HBHA(CBCACO)NH, C(CCO)NH, H(CCO)NH) in conjunction with 3D ^{15}N-separated, ^{13}C-separated, and ^{13}C/^{13}C-separated NOE experiments.[19] Side-chain torsion angle restraints within the active site loop were derived from short mixing time 3D ^{13}C-separated NOE spectra recorded in $^{2}H_2O$ and H_2O.[19] Loose backbone torsion angle restraints were derived from backbone ^{15}N, $^{13}C^{\alpha}$, $^{13}C'$, $^{13}C^{\beta}$ and $^{1}H^{\alpha}$ chemical shifts using the program TALOS.[20]

Residual dipolar couplings

$^{1}D_{NH}$, $^{1}D_{NC'}$ and $^{2}D_{HNC'}$ RDCs were obtained by taking the difference in the corresponding *J* couplings measured in aligned and isotropic (water) media.[21] The $^{1}J_{NH}$ couplings were determined from a 2D in-phase/anti-phase ^{1}H–^{15}N HSQC spectrum, and $^{1}J_{NC'}$ and $^{2}J_{HNC'}$ couplings were measured from a transverse relaxation optimized (TROSY)-based carbonyl-coupled ^{1}H–^{15}N HSQC spectrum. Three alignment media were employed: 18 mg/ml of phage pf1[22,23] with the addition of 0.5 M NaCl to eliminate line-broadening arising from attractive electrostatic interactions between the protein and negatively charged phage; and axially stretched[24] neutral and positively charged polyacrylamide gels. The neutral gel, prepared as described,[25] was made from 5% (w/v) polyacrylamide (39:1 (w/w) acrylamide/bisacrylamide), and positive charges were introduced by replacing 5% of the volume of acrylamide used in the polymerization reaction by diallyldimethylammonium chloride. The dried gels were soaked with protein solution for two days prior to transfer to NMR tubes. Alignment tensors and their scalar products[9] were determined by best-fitting the measured RDCs to the coordinates of the previously determined structure of unphosphorylated IIB^{Mtl} by singular value decomposition using the program Xplor-NIH.[26]

$^{3}J_{NP}$ couplings

$^{3}J_{NP}$ coupling constants were measured by quantitative *J*-correlation spectroscopy using two constant-time ^{1}H–^{15}N HSQC spectra (100 ms acquisition time in the indirect ^{15}N dimension) collected in an interleaved manner in the presence or absence of ^{31}P decoupling during the constant-time evolution period.[14]

Structure calculations

NOE-derived interproton distance restraints related specifically to residues in the active site loop (residues 383–393) were classified into loose approximate distance ranges of 1.8–2.7 Å, 1.8–3.5 Å, 1.8–5.0 Å and 1.8–6.0 Å corresponding to strong, medium, weak and very weak NOE cross-peak intensities, respectively; an additional 0.5 Å was added to the upper distance bound of distance restraints involving methyl groups; NOEs involving non-stereospecifically assigned methyl, methylene and aromatic protons were represented by a $(\Sigma r^{-6})^{-1/6}$ sum. The error range employed for χ_1 torsion angle restraints (represented by square-well potentials) was $\pm 20°$ when a unique rotamer could be identified.

Structures were calculated using torsion angle simulated annealing[27] with the program Xplor-NIH.[26] Only the coordinates of the active site loop (residues 383–393) were allowed to move. The remaining coordinates were held fixed to their positions in the previously determined structure of IIB^{Mtl}.[4] The minimized target function comprised the experimental NMR restraints (NOE-derived interproton distances, torsion angles and residual dipolar couplings), a quartic van der Waals repulsion term for the non-bonded contacts, and a multi-dimensional torsion angle database potential of mean force.[28] Structure Figures were generated using the program VMD-XPLOR.[29]

Protein Data Bank accession code

The atomic coordinates and experimental NMR restraints have been deposited in the Protein Data Bank Research Collaboratory for Structural Bioinformatics, Rutgers University, New Brunswick, NJ† with PDB accession code 1VRV.

Acknowledgements

We thank Drs David Williams and Alan Peterkofsky for useful discussion, Drs Dan Garrett and Frank Delaglio for software and technical support, and Dr Alan Peterkofsky for the clone of enzyme I. This work was supported, in part, by the AIDS Targeted Anti-Viral Program of the Office of the Director of the National Institutes of Health (to G.M.C.).

References

1. Robillard, G. T. & Broos, J. (1999). Structure/function studies on the bacterial carbohydrate transporters, enzymes II, of the phosphoenolpyruvate phosphotransferase system. *Biochim. Biophys. Acta*, **1422**, 73–104.
2. Van Weeghel, R. P., Meyer, G. H., Pas, H. H., Keck, W. & Robillard, G. T. (1991). Cytoplasmic phosphorylating

† http://www.rcsb.org

domain of the mannitol-specific transport protein of the phosphoenolpyruvate-dependent phosphotransferase system in *Escherichia coli*: overexpression, purification, and functional complementation with the mannitol binding domain. *Biochemistry*, **30**, 1774–1779.
3. Cornilescu, G., Lee, B. R., Cornilescu, C. C., Wang, G., Peerkofsky, A. & Clore, G. M. (2002). Solution structure of the phosphoryl transfer complex between the cytoplasmic A domain of the mannitol transporter $II^{Mannitol}$ and HPr of the *Escherichia coli* phosphotransferase system. *J. Biol. Chem.* **277**, 42289–42298.
4. Legler, P. M., Cai, M., Peterkofsky, A. & Clore, G. M. (2004). Three-dimensional solution structure of the cytoplasmic B domain of the mannitol transporter $II^{Mannitol}$ of the *Escherichia coli* phosphotransferase system. *J. Biol. Chem.* **279**, 39115–39121.
5. Zhang, M., Zhou, M., van Etten, R. L. & Stauffacher, C. (1997). Crystal structure of bovine low molecular weight phosphotyrosyl phosphatase complexed with the transition state analog vanadate. *Biochemistry*, **36**, 15–23.
6. Ab, E., Shuurman-Wolters, G. K., Nijlant, D., Dijkstra, K., Saier, M. H., Robillard, G. T. & Scheek, R. M. (2001). NMR structure of the cysteinyl-phosphorylated enzyme IIB of the *N*,*N*′-diacetylchitobiose-specific phosphoenolpyruvate-dependent phosphotransferase system of *Escherichia coli*. *J. Mol. Biol.* **308**, 993–1009.
7. Pannifer, A. D. B., Flint, A. J., Tonks, N. K. & Barford, D. (1998). Visualization of the cysteinyl-phosphate intermediate of a protein-tyrosine phosphatase by X-ray crystallography. *J. Biol. Chem.* **274**, 10454–10462.
8. Otten, R., van Lune, F. S., Dijkstra, K. & Scheek, R. M. (2004). ^{1}H, ^{13}C and ^{15}N resonance asignments of the phosphorylated enzyme IIB of the mannitol-specific phosphoenolpyruvate-dependent phosphotransferase system of *Escherichia coli*.. *J. Biomol. NMR*, **30**, 461–462.
9. Sass, J., Cordier, F., Hoffman, A., Rogowski, M., Cousin, A., Omichinski, J. G. *et al*. (1999). Purple membrane induced alignment of biological macromolecules in the magnetic field. *J. Am. Chem. Soc.* **121**, 2047–22055.
10. Clore, G. M. & Garrett, D. S. (1999). *R*-factor, free *R* and complete cross-validation for dipolar coupling refinement of NMR structures. *J. Am. Chem. Soc.* **121**, 9008–9012.
11. Williams, D. C., Cai, M. & Clore, G. M. (2004). Molecular basis for synergistic transcriptional activation by Oct1 and Sox2 revealed from the solution structure of the 42-kDa Oct1·Sox2·*Hoxb1*-DNA ternary transcription factor complex. *J. Biol. Chem.* **279**, 1449–1457.
12. Williams, D. C., Cai, M., Suh, J.-Y., Peterkofsky, A. & Clore, G. M. (2005). Solution structure of the 48-kDa $IIA^{Mannose}$-HPr complex of the *Escherichia coli* mannose phosphotransferase system. *J. Biol. Chem.* **280**, 20775–20784.
13. Dingley, A. J. & Grzesiek, S. (1998). Direct observation of hydrogen bonds in nucleic acid base pairs by internucleotide $^{2}J_{NN}$ couplings. *J. Am. Chem. Soc.* **120**, 8293–8297.
14. Mishima, M., Hatanaka, M., Yokoyama, S., Ikegami, T., Wälchi, M., Ito, Y. & Shirakawa, M. (2000). Intermolecular ^{31}P–^{15}N and ^{31}P–^{1}H scalar couplings across hydrogen bonds formed between a protein and a nucleotide. *J. Am. Chem. Soc.* **122**, 5883–5884.
15. Laskowski, R. A., MacArthur, M. W., Moss, D. S. & Thornton, J. M. (1993). PROCHECK: a program to check the stereochemical quality of protein structures. *J. Appl. Crystallog.* **26**, 283–291.
16. Reddy, P., Fredd-Kuldell, N., Liberman, E. & Peterkofsky, A. (1991). Overproduction and rapid purification of the phosphoenolpyruvate:sugar phosphotransferase system proteins enzyme I, HPr and protein III^{Glc} of *Escherichia coli*. *Protein Expr. Purif.* **2**, 179–187.
17. Delaglio, F., Grzesiek, S., Vuister, G. W., Zhu, G., Pfiefer, J. & Bax, A. (1995). NMRPipe: a multidimensional spectral processing system based on UNIX pipes. *J. Biomol. NMR*, **6**, 277–293.
18. Garrett, D. S., Powers, R., Gronenborn, A. M. & Clore, G. M. (1991). A common sense approach to peak picking two-, three- and four-dimensional spectra using automated computer analysis of contour diagrams. *J. Magn. Reson.* **95**, 214–220.
19. Clore, G. M. & Gronenborn, A. M. (1998). Determining the structures of large proteins and protein complexes by NMR. *Trends Biotechnol.* **16**, 22–34.
20. Cornilescu, G., Delaglio, F. & Bax, A. (1999). Protein backbone angle restraints from searching a database for chemical shift and sequence homology. *J. Biomol. NMR*, **13**, 289–302.
21. Bax, A., Kontaxis, G. & Tjandra, N. (2001). Dipolar couplings in macromolecular structure determination. *Methods Enzymol.* **339**, 127–174.
22. Clore, G. M., Starich, M. R. & Gronenborn, A. M. (1998). Measurement of residual dipolar couplings of macromolecules aligned in the nematic phase of a colloidal suspension of rod-shaped viruses. *J. Am. Chem. Soc.* **120**, 10571–10572.
23. Hansen, M. R., Rance, M. & Pardi, A. (1988). Observation of long-range ^{1}H–^{1}H distances in solution by dipolar coupling interactions. *J. Am. Chem. Soc.* **120**, 10571–10572.
24. Saas, H. J., Musco, G., Stahl, S. J., Wingfield, P. T. & Grzesiek, S. (2000). Solution NMR of proteins within polyacrylamide gels: diffusional properties and residual alignment by mechanical stress or embedding of oriented purple membranes. *J. Biomol. NMR*, **18**, 303–309.
25. Ulmer, T. S., Ramirez, B. E., Delaglio, F. & Bax, A. (2003). Evaluation of backbone proton positions and dynamics in a small protein by liquid crystal NMR spectroscopy. *J. Am. Chem. Soc.* **125**, 9179–9191.
26. Schwieters, C. D., Kuszewski, J., Tjandra, N. & Clore, G. M. (2003). The Xplor-NIH NMR molecular structure determination package. *J. Magn. Reson.* **160**, 65–73.
27. Schwieters, C. D. & Clore, G. M. (2001). Internal coordinates for molecular dynamics and minimization in structure determination and refinement. *J. Magn. Reson.* **152**, 288–302.
28. Clore, G. M. & Kuszewski, J. (2002). χ_1 rotamer populations and angles of mobile surface side chains are accurately predicted by a torsion angle database potential of mean force. *J. Am. Chem. Soc.* **124**, 2866–2867.
29. Schwieters, C. D. & Clore, G. M. (2001). The VMD-XPLOR visualization package for NMR structure refinement. *J. Magn. Reson.* **149**, 239–244.

Edited by M. F. Summers

(Received 6 July 2005; accepted 13 September 2005)
Available online 28 September 2005